Proceedings of the ASME 2023
International Design Engineering Technical Conferences and
Computers and Information in Engineering Conference
IDETC-CIE2023
August 20-23, 2023, Boston, Massachusetts

DETC2023-116842

GENERATING LARGE DATASETS OF SIMPLIFIED AUTOMOTIVE BODY-IN-WHITE STRUCTURES TO PREDICT SPRINGBACK USING MACHINE LEARNING

Abhishek Lokesh Bolar
The Ohio State University
Columbus, OH

Ibraheem Alawadhi
The Ohio State University
Columbus, OH

Satchit Ramnath*
The Ohio State University
Columbus, OH

Prakash Kumar
Arizona State University
Tempe, AZ

Yannis Korkolis
The Ohio State University
Columbus, OH

Joseph K. Davidson
Arizona State University
Tempe, AZ

Jami J. Shah
The Ohio State University
Columbus, OH

ABSTRACT

Automotive structures are primarily made of flexible sheet metal assemblies. Flexible assemblies are prone to manufacturing variations like springback which may be caused due to non-isotropic material properties from cold rolling, springback in the forming process, and distortion from residual stresses when components are clamped, and spot welded. This paper describes the curation of a large data set for machine learning. The domain is that of flexible assembly manufacturing in multi stages: component stamping, configuring components into sub-assemblies, clamping and joining. The dataset is generated by nonlinear FEA. Due to the size of the data set, the simulation workflow has been automated and designed to produce variety and balance of key parameters. Simulation results are available not just as raw FE deformed (sprung back) geometries and residual stresses at different manufacturing stages, but also in the form of variation zones and fits. The NUMISHEET 1993 U-draw/bending was used a reference for tooling geometry and verification of the forming process. Additional variation in the dataset is obtained by using multiple materials and geometrical dimensions. In summary, the proposed simulation method provides a means of generating a design space of flexible multi-part assemblies for applications such as dataset generation, design optimization, and machine learning.

Keywords: data curation, sheet metal, springback, forming, stamping, joining, automated workflow, finite element analysis, dataset generation

1. INTRODUCTION

The production of large assemblies, such as automotive bodies shown in Figure 1, involves flexible components like sheet metal stampings. The assembly process comprises numerous flexible subassemblies that are joined progressively, with each subassembly being built in a similar progressive manner, as illustrated in Figure 2. It is common for two individually stamped parts to exhibit slight mismatches when they are brought together for joining into subassembly demanding special tooling and clamping to achieve proper alignment. Consequently, accurately predicting and controlling the gaps between the adjacent assemblies becomes a necessity. Moreover, the inaccuracy in alignment accumulates further as subassemblies of parts are stacked highlighting the importance of a holistic simulation approach that considers multiple disciplines including material science, structural design and analysis, forming mechanics, 3D tolerance analysis, and assembly design.

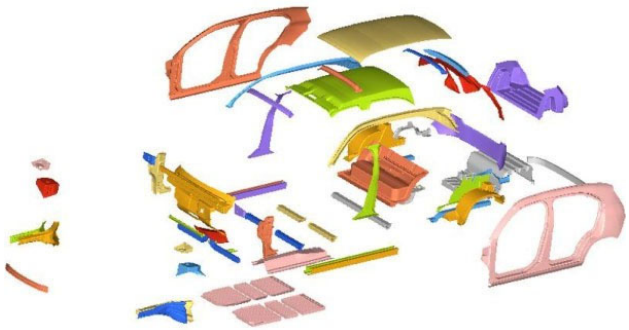

FIGURE 1: A COMPLEX FLEXIBLE ASSEMBLY [1]

* Corresponding Author: ramnath.17@osu.edu

At the end of the forming process when the component is released from the tool and die forces, springback occurs. It is defined as the geometric change the component experiences upon completion of plastic deformation from sheet metal forming when the aforementioned forces are released. Springback can lead to inaccurate dimensional precision in the finished component. This phenomenon is often undesired as it results in increased geometric variability for subsequent forming operations and assemblies. The use of Advanced High Strength Steels (AHSS), including Dual Phase (DP), Mild Steel (MS), and Transformation Induced Plasticity (TRIP) grades in cold rolled form, produces anisotropic properties and variable sheet thickness, leading to complex or inadequate material models that exacerbate the challenge of predicting springback. This issue is common in the automotive industry. Often dies must be re-machined several times in order to get the right shapes by trial and error [2].

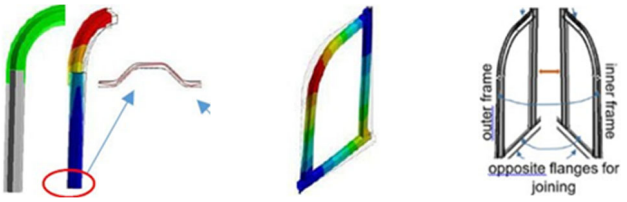

Simple Assembly | Closed Loop Assembly | Matched Pair Assembly

FIGURE 2: FLEXIBLE ASSEMBLY PROCESS

1.1 Research Goal

The trial-and-error procedures used in practice today are costly and time consuming often leading to delays in new product launch and quality problems. These drawbacks can be reduced or eradicated through the utilization of Artificial Neural Nets (ANN). Once trained and validated, they provide the potential for expeditious data-driven design space exploration. Although generating the required data requires significant initial investment, by a combination of simulations and testing, the benefits are worthwhile in the long run since the design space is exhaustively explored yielding not only better designs but also enabling the retrieval of some previously "rejected" designs for new designs. This research proposes a method to curate large datasets, at various stages from individual stamping to assembly, for training a set of ANN algorithms to collaborate and predict the final outcome. The datasets are curated via a multi-stage simulation workflow encompassing component stamping and component joining from subassemblies and assemblies. Automotive body structures, such as the one illustrated in Figure 1, provide a real-world application. The creation of these hollow structures involves joining the subassemblies of two matched (and opposite) hat sections at the flanges, which in turn are made by joining stamped hat-section components end-to-end (Figure 2). The test case used in this study is a simplified T-joint similar to the one found in the lower B-pillar region where the B-pillar joins with the side sill as shown in Figure 3.

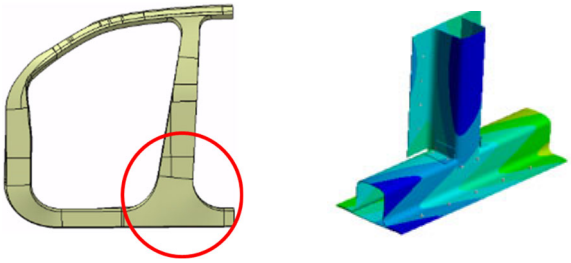

(a) (b)

FIGURE 3: (a) LOWER B-PILLAR JOINT ON AN AUTOMOTIVE DOOR RING (b) SIMPLIFIED T-JOINT

2. BACKGROUND

With the rapid increase in computation power, finite element methods (FEM) for analyzing and predicting springback have become more attractive. Various benchmark tests [1][3][4] illustrate the state of the art in predicting springback with FEM.In particular, the 1993 benchmark [1] represents a flanged channel forming operation that was simulated using FEM, whose results were compared to experimental results.

To investigate the physical and numerical sensitivity of sheet springback simulations, draw-bend tests are analyzed using finite element modeling. The draw-bend test is chosen as a well-characterized example of a forming operation that produces spring back similarly to industrial press forming operations. The test mimics closely the mechanics of deformation of sheet metal as it is drawn, stretched, bent, and straightened over a die radius entering a typical die cavity. As such, it represents a wide range of sheet-forming operations, and has the advantage of simplicity [5].

2.1 Data Curation

The performance of a machine learning (ML) algorithm is limited by various factors of the data sets used in training like quality, quantity, validity, and balance. For sales and business applications, large data sets are already available. In recent years, a few datasets have been generated for training ANNs in the engineering domain. The most common ones are the Modified NIST [6] and the Fashion-MNIST [7]. The MNIST and Fashion-MNIST datasets contain images of numbers and clothing apparels respectively. Neither dataset contain data suitable for the mechanical engineering domain.

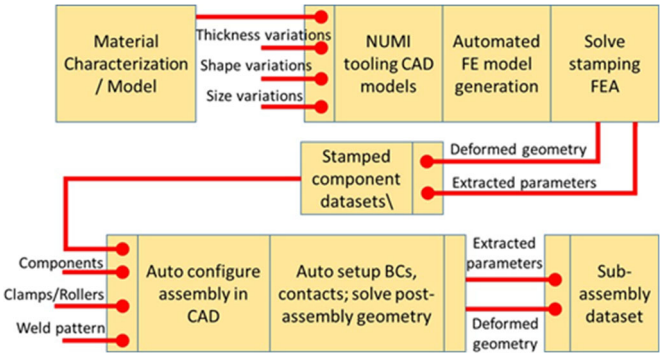

FIGURE 4: FLOWCHART FOR DATA GENERATION

For engineering design applications, data with higher resolutions, greater modality, and parameterization are required for learning useful relationships. However, these datasets inherently tend to be more customized to one specific application, making the tasks of generating and curating the data required for each unique design space. One such example is BIKED, from Regen wetter et al. [8], which includes assembly images, component images, design parameters, and labels for 4,500 unique bicycle designs. While BIKED is novel and useful in the realm of bicycle design, the dataset does not include results from analyses such as structural integrity and tolerance analysis. However, the volume and variety of data needed to train ANNs for design and performance (e.g., structural integrity) are limited like [9][10] generated using methods described in [11] and [12].

For developing and training an ANN for sheet metal stamping the dataset has to be curated and validated. That includes devising an integrated simulation pipeline for multi-stage process and automating multi-stage simulation in order to produce large enough data sets for training. The flowchart (Figure 4) outlines the main aspects of the data generation pipeline.

2.2 Current State of Art in Multi-stage Simulation

In order to investigate the physical and numerical sensitivity of sheet springback simulations, draw-bend tests are analyzed using FEA. The draw-bend test is chosen as a well-characterized example of a forming operation that produces spring back similarly to industrial press forming operations [13]. The test mimics closely the mechanics of deformation of sheet metal as it is drawn, stretched, bent, and straightened over a die radius entering a typical die cavity. As such, it represents a wide range of sheet forming operations, and has the advantage of simplicity [5].

Tolerance analysis in assemblies held the assumption that parts were rigid bodies; traditional methods did not account for the potential for deformation when using flexible components, such as those formed from sheet metal [14]. Liu et al. modeled parts as linear springs in series or parallel, which is only applicable to simple 1D stacks [15]. Camelio et al. demonstrated a more elaborate treatment where linear FEA is used to determine key point deformations. In order to reduce the number of variables, the authors classified surface "deformation patterns" into a small number of typical patterns seen in manufacturing (convex, concave, single wave), and used Principal Component Analysis (PCA) to extract those patterns from "simulated" measurements of individual components in their free state [16].

Advances and improvements in these methods have been presented by Merkley et al. [17], Ceglarek and Shi [18], Mortensen [19], Tonks and Chase [20][21]. Some of the limitations in these methods are (i) the focus was on 1D variations and focused on component failure rates rather than tolerance analysis, (ii) all components were simplified significantly, hence, local manufacturing variations cannot be considered, (iii) the process of analyzing tolerances is cumbersome since it does not directly relate to tolerancing standards such as ASME Y14.5 [22], and (iv) the models were developed for assembling two nominally flat sheets and is difficult to generalize for use in more realistic flexible assemblies.

In more recent years, Stockinger et al. [23] addressed the over-simplification of past models by using FEA to simulate variations of a stamped component (a cross-shaped bowl in 3D featuring springback), then position combinations of two components together at a time in computer-aided tolerancing (CAT) software and measure gaps between flanges. However, the study does not include an examination of the forces required to close the measured gaps and deformation following assemblies' joining/release was not considered. Moos and Vezzetti [24] focused on the fixturing and spot welding of variable 3D components in butt joints and slip joints using multi-stage simulation. The results include assembly- level springback results and assembly-level manufacturing variations but lacks a forming simulation stage to generate the component-level variations. In 2017, Hashemian and Imani [25] considered the last assembly step in attaching automotive roofs welded to a rigid frame. The authors compared coordinate-measuring machine (CMM) data to Monte Carlo models of curvature variations of the roof. In recent years commercial GDT tools, such as 3DCS and VisVSA, have incorporated FEA for flexible assembly variability analysis. However, this is an accurate method of generating the assembly-level manufacturing variations, but still uses only pre-defined parametric representations of the component variations as opposed to performing both stamping and assembly simulations in series.

From these reviews, it can be concluded that predicting variability in flexible assemblies, such as automotive body structures, remains an unsolved problem, despite the economic benefits it can yield for industry. Studies so far are limited in several ways: in their scope, (to one or two stages in the process chain); in the range of variables considered (material, tooling, work piece, dimensional and geometric parameters); and in

over- simplified shapes. The diverse slices in dealing with each of these aspects cannot be integrated because of incompatible models and impractical scalability. A holistic approach is needed that considers the entire pipeline, from AHSS anisotropy to component variability to multistage assembly and joining variability. Traditional approaches to solving this problem, suchas DOE cannot handle the number of variables. Given the non-linearities in the material, process, and simulations, neural networks would be the most suitable approach since they are non-linear analysis tools that form a highly interconnected, parallel computation structure with several simple processing elements, or neurons. Viswanathan et al, used a neural network control system, along with a stepped binder force trajectory, to control the springback angle in a steel channel forming process [26]. However, the method was demonstrated using a simple channel geometry (component) that used only a few input and output parameters. The method proposed in this paper considers a lot more input and output parameters, not just on the component level, but also in the assemblies. Hence, the result is a much larger network of non-linearities among various parameters in the model.

3. SIMULATION WORKFLOW

To generate the volume of data needed for this investigation, a multi-stage explicit finite element simulation workflow has been developed. In addition to the simulation workflow itself, methods for extracting, processing, and curating key results from the simulations have been applied. The following sections outline the overall scope of the workflow, the verification of the forming simulation using existing benchmarks [1][27], the organization and modeling procedure of each simulation in the workflow, and the extraction, processing, and curation of the results.

3.1 Scope of Workflow

The simulation workflow consists of three separate but co-dependent explicit finite element analysis stages. At a high level, the workflow simulates forming of two individual geometrically unique hat sections (the vertical and the horizontal components) followed by the joining of these components with flat sheets and brackets as shown in Figure 5.

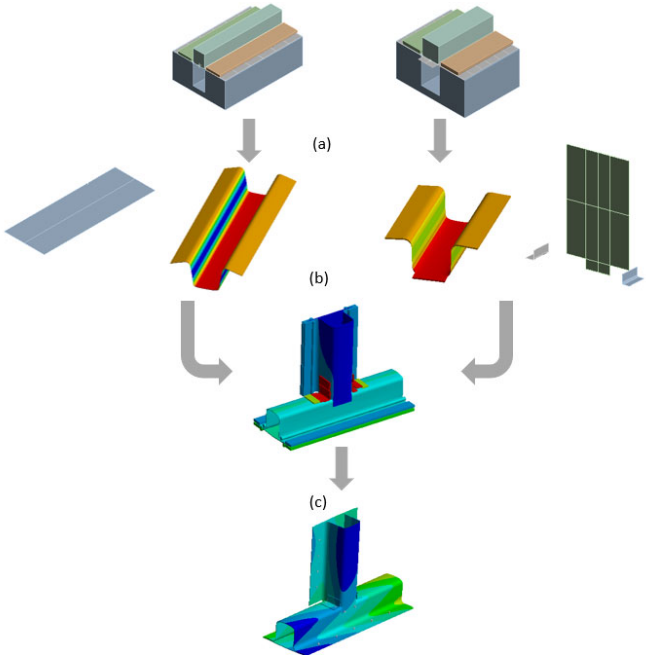

FIGURE 5: OVERVIEW OF SIMULATION WORKFLOW

Utilizing the NUMISHEET 1993 2D U-draw/bending benchmark [1] for its tooling geometry and forming process as well as the material properties used in a different investigation [27], the first analysis stage as seen in Figure 5(a) simulates the forming and spring back of the vertical and horizontal components from blank sheets. At this point, a wide variety of components are produced to be used in additional assemblies using modifications in tooling geometry, process parameters, and materials.

The second analysis stage as seen in Figure 5(b) involves the selection of a vertical formed component and a compatible horizontal formed component and clamping them together with flat sheets and brackets to prepare them for the joining process. Since this simulation stage requires inputs from two separate forming simulations, the deformed meshes and associated stresses/strains are imported from the first stage and transformed into the clamping arrangement as illustrated in Figure 5. At this point, the pair of vertical and horizontal components are varied keeping in check of the compatibility between both the components to create multiple assembly configurations.

The deformed meshes and the associated stresses and strains from the clamping simulation must be carried over to the joining stage as well. This stage involves the addition of spot welds between the flanges of the vertical/horizontal components and the flat sheet. Similar spot welds are also added between the components and brackets. Once the spot welds are in place, the clamps are released to allow the assembly to deform based on the residual stresses that were carried over from the forming and clamping simulations.

Once all the three stages of simulation are complete, results of engineering relevance are extracted. Directional deformations along pre-defined paths/edges are extracted from the FE simulation results and are subsequently transformed into parameters that describe post forming spring back and post joining twist. These findings as well as some important input parameters like material properties, geometric parameters are organized into a dataset that connects the workflow's input and output parameters. This way the dataset and its structure can be used to train and develop ANN's in the future. In addition to this, the workflow is parametrized at various stages to allow automation in future, which could produce even larger datasets in comparably less time than manually running each simulation.

3.2 Forming Simulation – Workflow Stage 1

The workflow for the forming simulation involves creating two straight hat sections which form the vertical and horizontal components, respectively. The vertical and horizontal components are geometrically quite different and require separate simulation setups. The horizontal component's geometric parameters, material properties, and FE model setup are obtained from a similar previous investigation [13], which is also based on the NUMISHEET [1] benchmark. The same organization for the simulation workflow is followed from [13], with the most apparent difference being the tooling geometry to accommodate for different hat section width and depth. The material model, element types, contact interactions, boundary conditions and hourglass controls were all identical. The deformed geometries and the residual stresses/strains are incorporated as inputs to the downstream clamping simulations as shown in Figure 5. Since the validation of this model was done previously in [13] against an existing set of experimental and simulated results [27] based on the NUMISHEET 1993 benchmark, and the overarching goal of this investigation is generating a curated dataset of flexible assembly data for application in future ANN training, additional changes were made to reduce the overall simulation time so that efficient automation of the workflow in the future can be done to create large sets of data. These changes include using larger element size (2.125 mm x 4.5 mm), a shorter forming process time of 0.105s and the introduction of mass scaling to meet a time step of 2.5e-0.6s. In this modified simulation the punch travels up to a depth of 50 mm in 0.04s, hold the position for 0.01s, raises to 50mm in 0.0175s, then moves up by 30mm in 0. 0125s.In the final 0.025s, the simulation allows the format hat section to spring back without any punch travel. After these changes, the solution time of the simulation reduces to 40 mins, which is a reasonable time keeping in mind the automation process to create a variety of components for the assembly configurations. The time steps are changed to match the punch travel speed and allow enough time for springback after the punch is out of contact from the other bodies.

The vertical component is also setup in the same way. It follows the same modelling techniques, has the same material model, but the geometry is changed. The overall length of the sheet is 182 mm, and a flange of 15 mm length and 45 mm width is included at one end of the hat section. This flange will be spot welded to the horizontal component during the assembly stage. The model organization, element type, hourglass controls, boundary conditions, contact interactions, process time is kept consistent with the horizontal component simulation. The setups for the vertical component and horizontal components are shown in Figure 6. The major difference between the vertical and horizontal components simulated in this case and the ones from [27] is the element size and type used for the blank sheets. This change affects the curvature in the sidewall due to springback and the bending/unbending over the die radius during the forming simulation. The solid bodies (i.e., punch, die and blanks) are modelled as rigid bodies as they are not required in the next stage of the workflow which is the clamping stage.

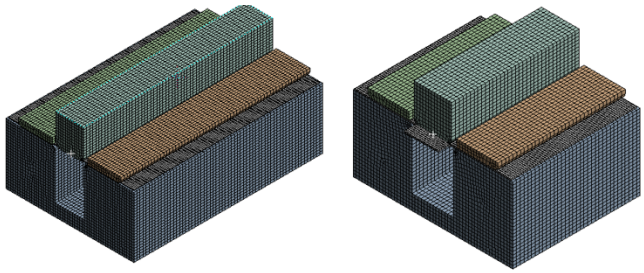

FIGURE 6: FORMING FINITE ELEMENT MODEL COMPONENT (A) HORIZONTAL (B) VERTICAL

The key results extracted from the horizontal and vertical simulations include directional deformations at multiple profiles along the length of the hat section (front, center and back) and the edges of the flanges (right and left). In addition to this, the key results from the vertical component also include the deformations along the bottom curved edges and the edges of the extended 15mm x 45mm flange. The profile deformations are extracted into excel spreadsheets and used to calculate several parameters defining the springback as stated in [1]. This topic is addressed in greater detail in section 4.

Variations to both geometry and material have been considered in the workflow for generating additional variety in the dataset. The geometric variations include changes in the section depth and width, sheet thickness, as well as changes to the tooling geometry. The material variations include modifications to the nominal materials (i.e., DP590, Aluminum Alloy) which include variations to the elastic modulus and stress strain curves. In the case of DP590 the stress strain values are provided using a table of values for plastic strain region (multilinear isotropic hardening). For the aluminum alloy, a tangent modulus for the bilinear isotropic hardening model is used. Table 1 shows the material properties of the two materials considered.

TABLE 1: MATERIAL PROPERTIES FOR SIMULATED DP590 STEEL AND AL ALLOY

Material	Density [Kg/mm3]	E [GPa]	Poisson's Ratio	Yield Strength [MPa]
DP590	7.85e-6	191	0.3	411
Al Alloy	2.70e-6	71	0.3	135

The subset of the variation in the forming simulation stage is shown in Table 2. The compatibility between the vertical component and horizontal component is pivotal for the assembly process and is explained in detail in Section 3.3.

TABLE 2: EXAMPLES OF VARIETY IN FORMING SIMULATION STAGE

Component	Material	Thickness [mm]	Width [mm]	Depth [mm]
Horizontal	DP590	1.5	45	50
Horizontal	Al	2.0	60	60
Vertical	DP590	2.0	50	48.0
Vertical	Al	1.5	55	63.5

3.3 Component Selection and Intermediate SolutionTransfer

On completion of the forming simulation, the next stage of the workflow involves selection of a vertical and horizontal component for the assembly stage with their intermediate solution (deformed mesh and residual stresses/strain values). The compatibility of the vertical and horizontal component is pivotal for the next stage of clamping simulation to run successfully. The components are put through a compatibility test such that the clamping simulations will only work if the difference between the hat section width and thickness of the vertical component is equal to the sum of the hat section depth and thickness of the horizontal component. In addition to this, the thickness and overall length of the flat sheet must be equal to their respective hat section component and width of the flat sheet must match the channel width and the flange width of their respective hat section components. Differences in the width of the vertical component and depth of the horizontal component are desirable to create additional variability in the dataset of the assembled components. In Table 2, the combination of DP590 horizontal and vertical components would be possible for assembly based on the compatibility check. The sum of the width and thickness of the horizontal component would be 46.0 mm and the difference of the depth and thickness of the vertical component would be 46.0 mm as well allowing this assembly to take place. Similarly, the combination of Al alloy horizontal and vertical components would be possible for assembly based on the compatibility check. The use of multiple materials allows for a greater variety in the dataset.

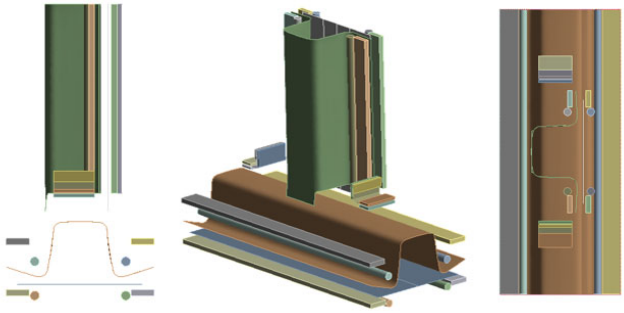

FIGURE 7: HORIZONTAL AND VERTICAL COMPONENTS WITH THEIR CORRESPONDING FLAT SHEET AND BRACKETS

In addition to the formed components, the flat sheets, brackets, and the clamps as seen in Figure 7 must be imported to the next stage of clamping simulation which will be discussed in detail in the next section. Once the correct compatible formed components are selected, each component's deformed mesh including the local thickness, residual stresses/strain, deformed meshes need to be imported to an intermediate external FE model where it is transformed (rotation and translation) to the required orientation for clamping simulation of the workflow. The associativity between mesh and the residual results is maintained by the intermediate model while allowing component transformations. This was achieved utilizing an external model system for each component and an imported *.k file created at the end of each component's forming simulation within the Ansys Workbench software program.

At the end of the clamping simulation, a similar *.k file is generated which serves as the input for the joining simulation process. The formed components, clamps, and brackets are exported to the next stage of joining through an external model.

3.4 Clamping Simulation – Workflow Stage 2

After compatible vertical and horizontal components are selected for the clamping stage and transformed into the right orientation with their residual stresses and deformed meshes, they must be clamped together to form a T joint with flat sheets and brackets so that simplified spot weld or rivets can be added to form the final assembly. In this workflow, the clamping occurs as a separate simulation from joining/release because of the modelling procedure followed in applying the spot welds. This will be discussed in detail in the next section. The clamping simulation requires input from four different intermediate FE models: two component models and two clamp models containing the flat sheets and brackets along with the solid rollers and clamps. The vertical clamp model has guide rollers and clamps along with the flat sheet for the vertical hat section and brackets and their clamps to join the vertical component and the horizontal component. The horizontal clamp model has the guide rollers and clamp along with the flat sheet for the horizontal hat section. The geometric parameters of this clamp model can be changed so that the same clamp model can be used to in all the clamping simulations by transforming the geometric parameters

based on the width and depth of the components to prevent initial penetrations post import. This structure of the clamp model significantly reduces the complexity of the simulation workflow. Figure 8 contains a description of the vertical and horizontal imported mesh model, clamp FE model, meshed brackets, and the flat sheet model.

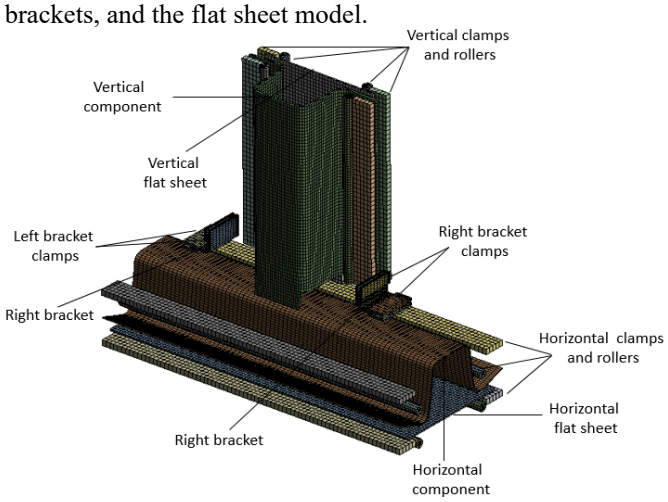

FIGURE 8: EXAMPLE OF MESH IMPORTED INTO CLAMPING SIMULATIONS

The clamps and guide rollers of the vertical and horizontal components work together to get the component flanges and the flat sheet in contact with each other by the end of the simulation. The solids used in the forming simulation are modelled as rigid bodies, while the solids used in the clamping simulations are modelled as flexible solid bodies. The latter are modelled as flexible solid bodies so that they are included in the mesh that is transferred to the joining simulation. The vertical and horizontal component clamps and rollers, the flat sheet, brackets, and the bracket clamps are modelled independently in their separate FE model before being imported to the clamping simulation. The cross-sectional data for the clamps and rollers are 5mm x 18mm rectangles and 8mm diameter circles, respectively, and their length is equal to the length of the corresponding hat sections. The width of the bracket clamps is 2.5 mm and are of varying breadth depending on the clamps. Their length is equal to the length of the brackets. The material models used for these solids are linear. Although the solids need to be modelled as flexible bodies so that the mesh data can be transferred to the joining simulation stage, they need to be rigid in their properties compared to the formed components. Consequently, they are modelled as structural steel with very high modulus of elasticity of 1000 GPa, poison's ratio of 0.3 and a density of 9000 Kg/m^3. The solids are meshed as LS-DYNA Type 1 linear hexahedral solid elements with a global size of 4mm. Different edge sizing is used based on the dimensions of the clamps to accurately represent the geometry of the solids. The material data and mesh model for the hat section components are retained from the forming simulation. The coefficient of friction between the sheets and solids and the sheets themselves is maintained at 0.10 so that the sheets can be held in place without inducing additional tangential contact stresses in the sheets. At the start of the simulation, the clamps and rollers move such that the vertical components are clamped with its corresponding flat sheet in 0.02s and they remain in this position till the end of the simulation (see Figure 8.) The horizontal clamps and rollers move and clamp the horizontal component with its flat sheet in 0.02s as well. These clamps are displaced to be exactly two sheet thicknesses apart. The horizontal clamps then settle down for a period of 0.07s. In this time period, the brackets move towards the vertical component and are clamped to the vertical component face. Once this process is completed, the horizontal clamps and rollers move the entire horizontal assembly up towards the vertical component assembly and create a single assembly. This happens over a time of 0.04s. In the remaining time of 0.03s, all the parts settle down and the total time of this assembly sums up to 0.16s. There are no additional boundary conditions applied on the sheets. Therefore, all the deformations in the sheet are due to their contact with the solids and with each other. Since this is a multi-level clamping simulation process, it takes almost 90 minutes to solve. At the end of the simulation a *.k file is generated which has all the deformed mesh, stresses/strains, for the solids and the components which is transferred to the joining stage through an external model system.

3.5 Joining Simulation – Workflow Stage 3

The final stage of the workflow is the joining simulation where the clamped model is joined by means of simple spot welds. The deformed mesh and the residual stresses for the solids and the components are imported from the previous clamping simulation stage. The spot welds are created between (i) the clamped flanges of the vertical and horizontal components with their corresponding flat sheets, (ii) the brackets and both the vertical and horizontal components, (iii) the vertical component's flange and horizontal component's face, and (iv) the vertical flat face with the horizontal component's face. The clamps and rollers are released which allows for assembly level deformations resulting from the buildup of residual stresses in each component. Since the model settings for the clamps, rollers and both the components are carried over from the clamping simulation, therefore creation of the spot welds is the most significant task at this workflow stage.

The locations of the spot welds must be decided before their simulation. The variation in weld pattern and the number of welds along the flanges gives additional variety in the assemblies generated. The weld pattern on the horizontal component is held constant with a total of five welds on each flange; such that there is one weld at the center of each flange and two others spread at a distance of 50 mm on both sides of the central weld as shown in Figure 9. The weld pattern on the vertical component is also held constant with four welds evenly spaced at 33 mm along the length of the flange. In addition to these welds, there are spot welds on the brackets joining them

with the vertical and horizontal component faces and welds between the vertical component's flange/vertical flat sheet's flange and horizontal component's face. There are a total of two welds separated by 35 mm on each on these brackets and flange faces (Figure 9).

The welds are modelled as body-to-body beam connectors of 2.5mm diameter cylinders with the same material properties as the rigid solid bodies, as described in Section 3.4. All the nodes falling within a 5.5 mm radius of the weld location of the respective sheets are coupled three dimensionally by the beam connectors. This allows stresses to be transferred between the beams without high concentration on the sheets, and the amount of affected material is similar to the size of an automotive body spot weld. This type of weld cannot be created during the simulation and needs to be created prior to the start of the simulation. Therefore, the joining and clamping simulations are two separate stages in the workflow.

This methodology of creating the spot welds as rigid connections between the sheets has its downside when it comes to creating variety in the design based on the sequence in which the assembly is done. Since they are rigid bodies, the mesh data of these welds are lost if they need to be transferred to another simulation stage. So, it would not be possible to create a simulation workflow where the horizontal component and vertical components are clamped and joined separately and then brought in to be joined together as the mesh data of these welds would be lost in the process. This limitation of the process can be addressed in the future.

After creating the spot welds, release of the clamps is modeled by reversing the contact interactions between the solids and the sheets and the sheets themselves, as described in Stage 2 (Section 3.4). The clamps and rollers are displaced and move away from the sheets in a time of 0.015s and the sheets are allowed to settle and deform due to the residual stresses from the clamping stage in 0.01s. Thus, the entire simulation of release ends in 0.025s with the simulation run time being 12 mins in total. At this point, the results from the assembly stage are ready to be extracted and more about this is explained in detail in the next section.

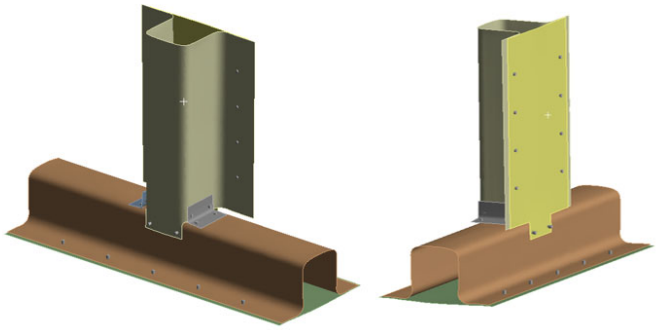

FIGURE 9: EXAMPLE OF THE WELD PATTERNS ON VARIOUS COMPONENTS OF THE ASSEMBLY

3.6 Results Extraction, Processing, and Curation

The important results of engineering significance may now be extracted from the deformed geometries following the simulation stage for both the horizontal and vertical components and the joining simulation stage for the assembly. These results are (a) the residual stresses and (b) the final coordinates of all nodal points from which the geometric shapes for both components (Section 3.2) and the full assembly (Section 3.5) in their free states may be determined. The procedure for extracting these data from the FE solutions, processing these data to produce results, and curating the results based on input parameters are covered in further detail in this section.

The solution within each model must be organized before the results are extracted from FE simulation stages. Key FE results for extraction include deformations along pre-defined paths within each model in both the forming and joining simulation stages. Examples of these path definitions are shown in Figure 10. For each path – defined prior to simulation execution, deformations in x, y and z direction are generated, which are then extracted into spreadsheets, allowing for calculationof the final positions of each node along the respective path.

These final positions may then be processed into the results set for the overall dataset generated by this workflow.

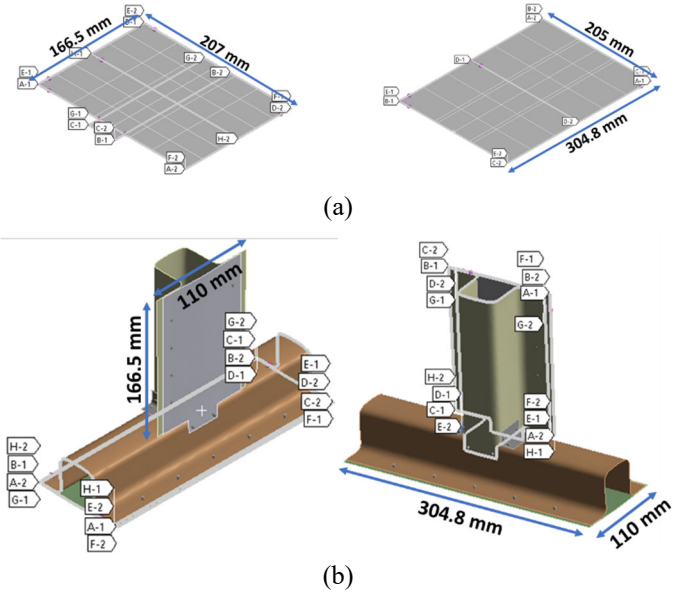

FIGURE 10: EXAMPLES OF PATHS DEFINED FOR FE RESULT EXTRACTION FROM A (a) AN UNDEFORMED BLANK AS A COMPONENT AND (b) AN ASSEMBLY

The FE simulation output data generated from the above paths must are processed into key results (examples are shown in section 4.1 and 4.2). The workflow inputs and outputs must be curated into a dataset in such a way that it can be used in training of future ANN's. The curation and organization method for this dataset involves the formulation of a theoretical multi-

dimensional matrix in which the value of each input parameter to the workflow provides one dimension in the matrix. This specific point in the multi-dimensional space corresponds to a unique set of outputs (based on ASU's results). The structure of this input matrix can be in the form of an indexed data structure within a specific program (less accessibility) or in in the form of nested folders (more accessibility) that an ANN algorithm can be trained to scan through during the training process.

4. RESULTS AND DISCUSSION

Using the methods described in Section 3.6 to generate, extract, and process results, a dataset has been prepared for curation and use in training of ANN algorithms. In this section, a subset of this dataset is shown as an example of the types of results generated by the workflow and available for curation. Also in this section is a description of the geometric parameters that may be used to evaluate the quality of a component or assembly for any given combination of input values used in the FE simulations.

4.1 Component-Level Results

In this section, a subset of the results are described for the stamped components that are used in the vertical and horizontal subassemblies. An example of the deformed geometry is shown in Figure 11 with a contour plot of residual stresses for a straight, 2.0 mm thick, 48 mm deep, 50 mm wide DP590 hat section which forms the horizontal component and a straight, 1.0 mm thick, 50 mm deep, and 45 mm wide DP590 hat section which form the vertical component generated from tooling in accordance with NUMISHEET [1] protocol. Figure 12 exhibits directional deformations available along a single path in these components. Each path becomes an exported result for additional processing into spring-back parameters.

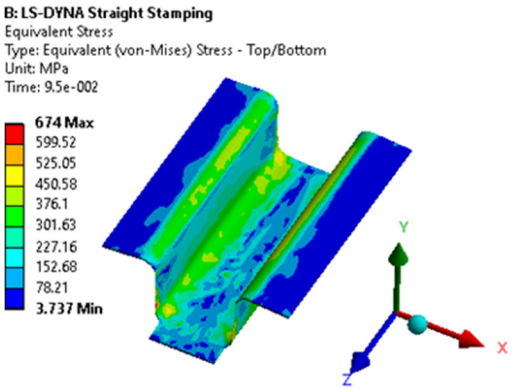

(a)

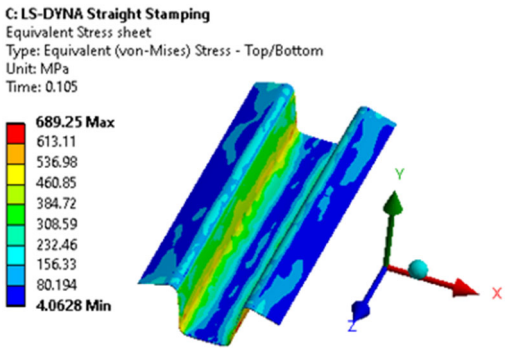

(b)

FIGURE 11: EXAMPLE OF DEFORMED GEOMETRY AND RESIDUAL STRESSES IN COMPONENTS (a) VERTICAL (b) HORIZONTAL

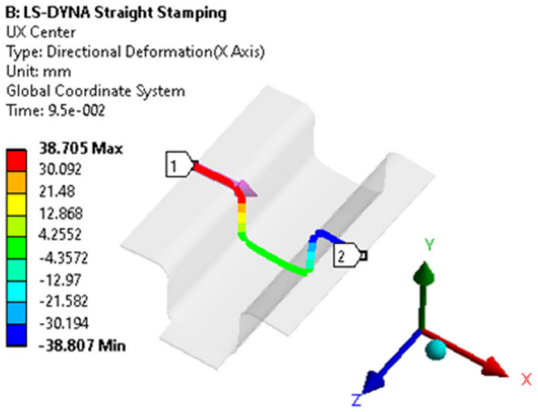

(a)

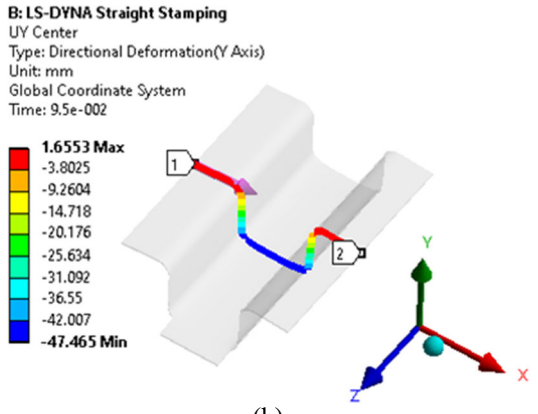

(b)

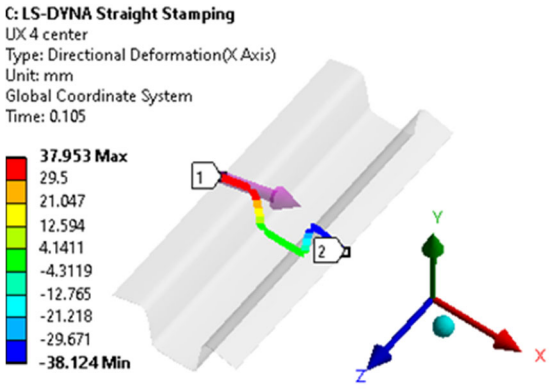

(c)

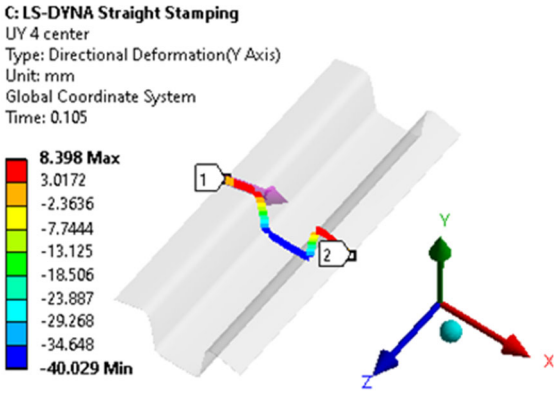

(d)

FIGURE 12: EXAMPLES OF X & Y DIRECTIONAL DEFORMATIONS ALONG A SINGLE PATH IN FORMED COMPONENTS (a & b) VERTICAL (c & d) HORIZONTAL

In the remainder of this section, we describe the geometric parameters that may be used to evaluate the geometry of stamped hat-section components in their free state. When a measured component is used in a welded assembly, the geometry of each component has influence on the quality of geometric shape of the welded assembly once it has been released from the fixture and spring-back deformation from residual stresses occurs. Two parameters we choose are the component angles that arise from the twist between two opposite long edges of a component. For instance, for the long edges of a hat component of the horizontal subassembly in Figure 12(d), the angles of twist are about the *x*- and *y*-axes.

The first step for calculating the twist angles between two nearly parallel edges of any component or assembly, is to obtain the least squares fit (LSF) line for each edge [28][29][30]. To do so, the mean of all the points along one edge is calculated using the NumPy [31] mean( ) method. The resulting mean is then subtracted from the data set of that edge. Then Singular Value Decomposition (SVD) is applied to the resulting shifted data set of each edge using the NumPy linalg.svd() method to calculate the direction vector of the line that best fit the data in the least squares sense [32]. Having these LSF directions, the second step is to project both onto two global coordinate frame planes, as shown for one LSF edge in Figure 13. There, the twist angle θ_t is the angular departure from the *z*-axis of the plane formed with the *x*-axis and normal vector **n** (the *x***n**-plane). Correspondingly, ϕ_t is the angular departure of the *y***n**-plane from the *z*-axis. The twist angles θ_t and ϕ_t for the one edge are obtained from the direction cosines *L*, *M*, and *N* of the straight-line least squares fit (LSF) of sprung-back nodal points along the edge, as represented in the global coordinate system. These are shown in Figure 13 with the dashed lengths obtained as the three projections from the unit vector along the LSF line onto the global *x*-, *y*-, and *z*-axes.

The angle θ_t for one edge may be found from two new direction cosines μ and ν that are derived from the dashed lines *M* and *N* in Figure 13: $(\mu, \nu) = (1/\rho)(M, N)$, where $\rho = \sqrt{M^2 + N^2}$. Then, $\theta_t = \text{arcsine}(\mu)$. Similarly, $\phi_t = \text{arcsine}(\lambda)$, where new direction cosine λ is obtained from $(\lambda, \nu) = (1/\rho)(L, N)$, and normalizing factor ρ now is $\rho = \sqrt{L^2 + N^2}$. Lastly, we compute the twist angle between *two* opposite edges of a component with $\theta_t = \text{arcsine}(\mu_2 - \mu_1)$ and $\phi_t = \text{arcsine}(\lambda_2 - \lambda_1)$. Then, each angle is converted from radians to degrees using the math.acos() and math.pi methods. An example of two LSFs to their data are shown in Figure 17.

Using the arcsine function allows for the possibility that one or both LSF lines could have a direction that lies in an octant other than the first.

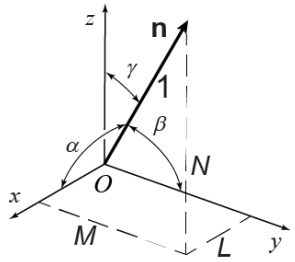

FIGURE 13: UNIT VECTOR IN THE DIRECTION OF THE LSF OF A STRAIGHT LINE THROUGH SPRUNG-BACK POINTS ALONG ONE EDGE OF A STAMPED COMPONENT. DASHED LINES ARE THE DIRECTION COSINES CORRESPONDING TO ANGLES α, β, AND γ.

4.2 Assembly-Level Results

In this section, the subset of results available at the assembly level are shown. The deformed geometry with the contour plots for residual stresses for an assembly of a straight, 2.0 mm thick, 48 mm deep, 50 mm wide DP590 hat section and 1.0 mm thick, 50 mm deep, and 45 mm wide DP590 hat section, generated in accordance with NUMISHEET tooling [1] with flat sheets and brackets are shown in Figures 14 and 15. Figure 15 shows the deformations along two single paths in the same assembly. These deformation displacements become exported results for additional processing into the assembly twist angles.

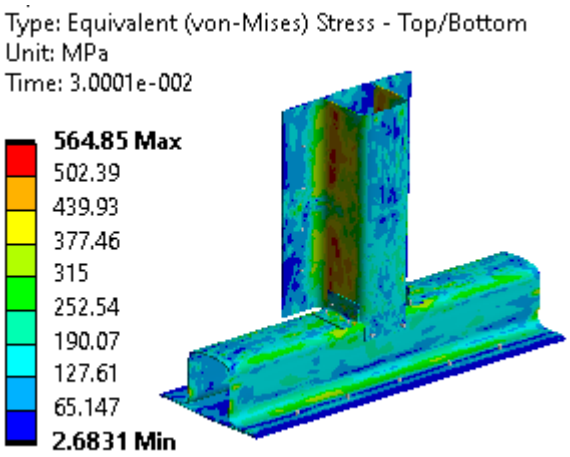

FIGURE 14: EXAMPLE OF DEFORMED GEOMETRY AND RESIDUAL STRESSES IN AN ASSEMBLY

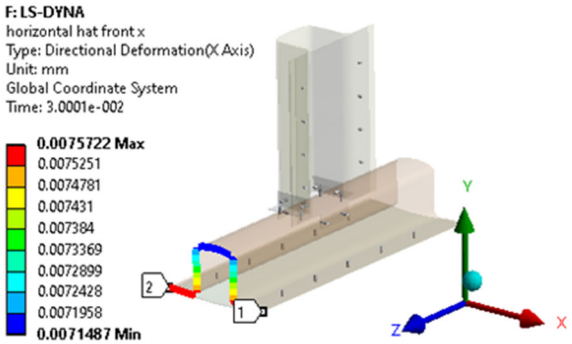

(a)

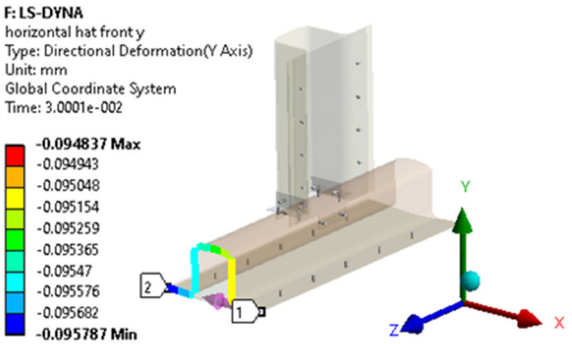

(b)

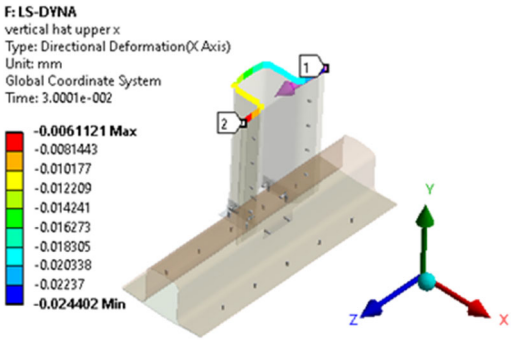

(c)

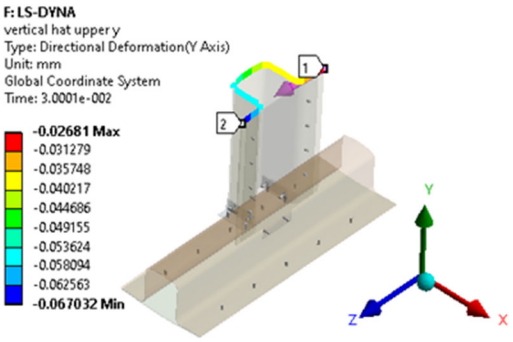

(d)

FIGURE 15: EXAMPLES OF DIRECTIONAL DEFORMATION ALONG DIFFERENT PATHS IN AN ASSEMBLY

The geometric sprung-back data that were extracted from a welded assembly, and to be used for geometric fitting, were all extracted from edges: the edges of the hat-section flanges, the end cross-sections of the hat-sections, and all four edges of the unstamped 'flat' components (Figure 16).

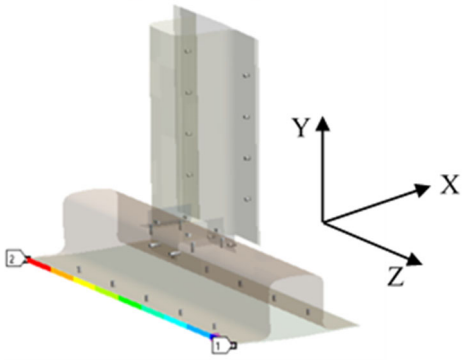

(a)

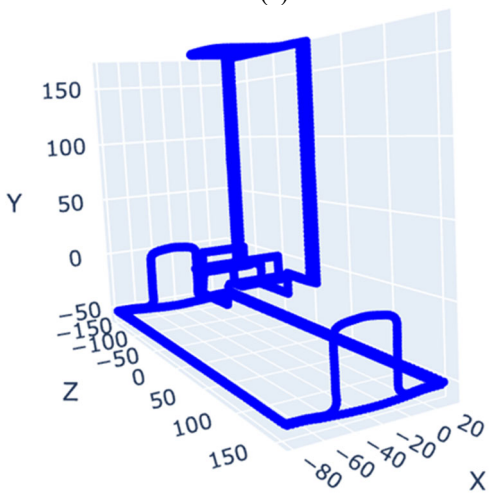

(b)

FIGURE 16: (a) THE AUTOMOTIVE T-JOINT ASSEMBLY FOR ONE SET OF INPUT VALUES. (b) LOCATIONS FOR THE SPRUNG-BACK POINT-DATA FOR THE ASSEMBLY IN (a).

At this time the geometric parameters for assessing assemblies are (A) unconstrained planar minimum-zone-magnitudes, (B) angles between fitted planes these zone fits, and (C) twist angles between two nearly parallel edges of an assembly. The method for computing the twist angles between edges is described in Sect. 4.1. The methods for computing the other two parameters are described in Subsections 4.2.1 and 4.2.2 below.

4.2.1. Unconstrained minimum zone magnitudes

For the unconstrained form zones, all the points from the flat sheets are used (Figure 10(a)), but data for the hat-sections are partitioned and only points along the flanges are used (Figs. 18(a) and 18(c)). Since the nodes used in all components of the FE simulations are located midway between the two surface boundaries of the sheet material, the half-thicknesses from both of the two joined components are included in the corresponding zone magnitudes.

The steps in computing the unconstrained minimum zones are [33]:

1. First, all the relevant points in the region for which the zone magnitude is to be determined are selected. These points should represent the components or assembly that are being analyzed.
2. The "ConvexHull()" function from the "scipy.spatial" [34] library is used to create a convex hull around the points in the data set. The origin must be interior to the hull.
3. The planar facets of the convex hull are identified, and, for each facet, the normal distance to each vertex in the hull is computed and the maximum one is selected and stored. Each normal distance from the origin is computed by calculating the cross product of two vectors formed from three points on the facet, and then finding the dot product of this normal vector with one of the points on the plane to get the distance.
4. The zone magnitude is obtained as the minimum value from the list of maximum distances from all the facets.

Examples of zone magnitudes and twist angles are shown in Table 3 and Table 4.

TABLE 3: TWIST ANGLES

Component/Assembly	Twist Angle (θ^0)	Twist Angle (φ^0)
Left and Right Edges of H.H	0.1242	0.1568
Left and Right Edges of H.S.	0.0428	0.0231
* H.H. – Horizontal Hat; H.S. – Horizontal Sheet		

TABLE 4: ZONE MAGNITUDES

Component/Assembly	Zone Magnitude (mm)
Horizontal Plane Sheet (A.A.)	2.7785
Horizontal Hat Sheet (A.A.)	1.7962
Vertical Plane Sheet (A.A.)	0.9999
Vertical Hat Flange (A.A.)	1.2457
Horizontal Hat and Plane Assembly	4.2106
Vertical Hat and Plane Assembly	2.3263
* A.A. – After Assembly	

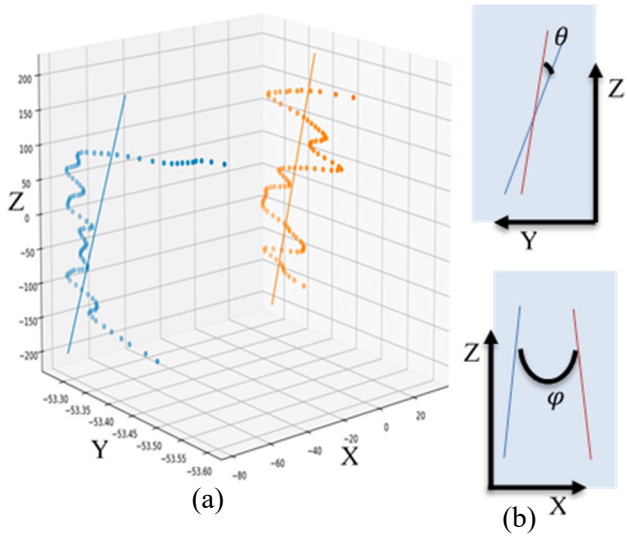

FIGURE 17: (a) DATA FROM TWO OPPOSITE EDGES OF A COMPONENT OR ASSEMBLY. (b) THE TWO PROJECTED ANGLES OF TWIST.

4.2.2. Angles between fitted planes

To estimate the perpendicularity of a T-joint, a plane is fitted to each of the (flat) unstamped components for the horizontal and vertical subassemblies of the fully assembled joint. This process involves collecting two sets of data from the horizontal and vertical components of the T-joint. The best-fit planes for each component are found by fitting the linear equation $ax + by + cz - 1 = 0$ to all points (x, y, z) that represent one of the respective planes PQRS or ABCD (Figure 18(a)). The pseudoinverse method [32] is used to find the coefficients a, b, and c for each best-fit plane. The normal vectors for both planes are calculated and named N1 and N2, respectively. To determine the relative rotation of the plane ABCD with respect to the plane PQRS in the global Z, X, and Y directions, three sets of angles are defined: α, β, and γ. A coordinate frame is fixed to the PQRS

plane so that PQRS is parallel to the global XZ plane (Figure 18(a)). To calculate the angle α, N1 is projected onto the XY plane, and the angle between the projected normal and the X axis is calculated. The angle α is then determined as this angle minus 90°. To calculate the angle β, a line is constructed through the midpoints of AB and CD and is projected onto the YZ plane. The angle β is determined as the angle between the projected line and the Y axis. Finally, to calculate angle γ, N1 is projected onto the XZ plane, and the angle γ is determined as the angle between the negative X axis and the projected line. The values of α, β, and γ are 87.97°, 0.041° and 0.097° respectively.

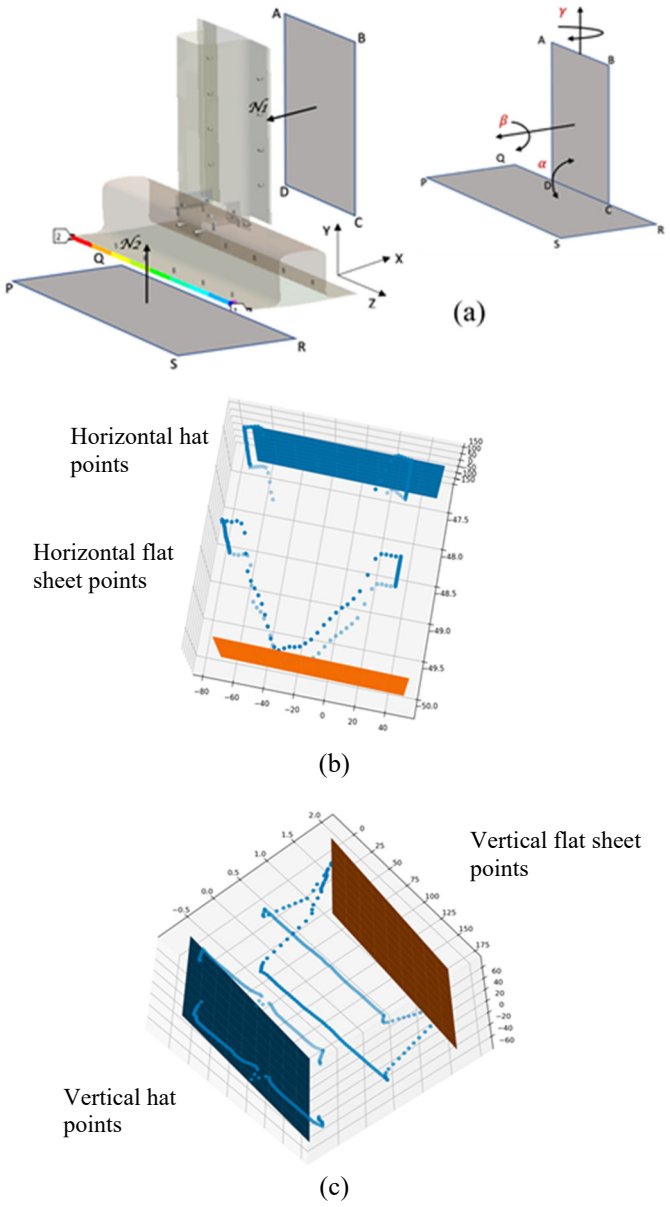

FIGURE 18: (a) THE ASSEMBLY SHOWING LOCATIONS OF POINTS FOR THE HORIZONTAL PLANAR ZONE FIT AND POINTS FOR THE VERTICAL PLANAR ZONE FIT. (b) POINTS FROM THE FLAT AND HAT-SECTION COMPONENTS AND THE RESULTING BOUNDARIES FOR THE HORIZONTAL PLANAR ZONE FIT. (c) POINTS FROM THE FLAT AND HAT-SECTION COMPONENTS AND THE RESULTING BOUNDARIES FOR THE VERTICAL PLANAR ZONE FIT.

4.3 Limitations

The presented workflow and its applications in training of ANNs comes with certain limitations to take into account. One limitation is the simplicity of the component shapes that have been generated thus far compared to the much more complex shapes used in real assemblies such as automotive bodies. Consequently, any algorithms trained would be restricted to making inferences solely based on the simple shapes generated in the current dataset. On the other hand, this limitation could be treated by extending the logic of this workflow to incorporate more complex shapes in future research obviating this limitation. Moreover, the springback parameters could be made more meaningful and elaborate, especially for assemblies.

Another limitation is the limited accuracy of the results in the current dataset that are affected by the specific simulations settings. Recalling when transitioning from the validating simulation to the simulation used for generating the dataset, the settings had to be modified which had noticeable effects on the springback being lower than expected. Therefore, any algorithm trained based on this dataset would be limited to only relative springback differences between components or relative twist differences between assemblies, as opposed to the absolute value of each. To rectify this issue, the validated forming simulation could be used to generate another dataset following the same workflow procedure, hence requiring additional computing time and power.

Additionally, a critical limitation for this workflow is neglecting the thermal effects in the heat affected zone caused by spot welding, which when compared to actual welded flexible assemblies has proved to be significant. To consider this phenomenon in the workflow would require additional simulations and models which are out of the scope of this work.

5. CONCLUSIONS

In conclusion, this work has produced an operational simulation workflow and post-processing scheme for generating a curated dataset of results significant for flexible assembly engineered products. The forming simulation was shown to utilize a validated process, the intermediate solutions from each simulation stage were properly transferred to downstream stages, and FE results were extracted and processed into geometric parameters for component spring back and for assembly deformations (twist and edge deviations). All of this allows for the curation of this data into a multi-dimensional matrix relating process inputs to key result outputs which, in turn, can be appliedto train future ANNs to predict the same results without the needfor simulation.

6. FUTURE WORK

Work is continuing to characterize additional geometric variations. For example, an additional geometric parameter for

the free-standing stamped components is the angle ϕ that is measured between the *zx*-plane and one of the flanges on a hat-section (Figure 19). (Symmetry inherent in the FE simulations causes the angle to be the same on both sides of a cross-section.) When the flanges are over-bent, they spring back in a completed assembly to produce a downward (rocking horse) bulge of the lower surface of the T-joint. This can be seen in the data of Figure 16(b). Including angle ϕ as a parameter would make it possible to ensure a stable datum at the undersurface of the T-joint. Additionally, machine learning algorithms are being developed to use the generated data and make multi-stage predictions for components and assemblies.

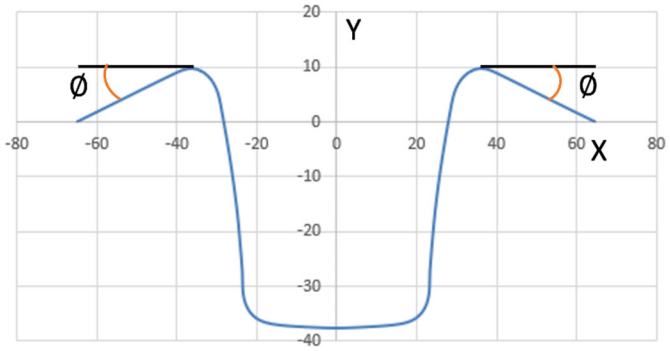

FIGURE 19: ANGLE ϕ THAT MEASURES THE DROOP OF THE FLANGES

ACKNOWLEDGEMENTS

The authors are grateful for funding provided to this project by National Science Foundation Award #2029905 and the technical support from Honda Development and Manufacturing of Americas LLC.

REFERENCES

[1] A. Makinouchi, E. Nakamchi, E. Onate, and R. Wagoner, "NUMISHEET '93," 1993.

[2] E. Mclaughlin, T. Gupta, A. Fallaharezadoor, and T. Altan, "Reducing springback in hat-shape bending with variable BHF using servo-hydraulic cushion," *Stamp. J.*, 2018.

[3] J. Lee, G. Kinzel, and R. Wagoner, "NUMISHEET '96," 1996.

[4] J. Gelin and P. Picart, "NUMISHEET '99," 1999.

[5] K. P. Li, W. P. Carden, and R. H. Wagoner, "Simulation of springback," *Int. J. Mech. Sci.*, vol. 44, no. 1, pp. 103–122, 2002.

[6] Y. LeCun, L. Bottou, Y. Bengio, and P. Haffner, "Gradient-based learning applied to document recognition," in *Proceedings of the IEEE*, 1998, vol. 86, no. 11, pp. 2278–2323.

[7] H. Xiao, K. Rasul, and R. Vollgraf, "Fashion-MNIST: a Novel Image Dataset for Benchmarking Machine Learning Algorithms," Aug. 2017.

[8] L. Regenwetter, B. Curry, and F. Ahmed, "BIKED: A Dataset for Computational Bicycle Design With Machine Learning Benchmarks," *J. Mech. Des. Trans. ASME*, vol. 144, no. 3, 2022.

[9] P. Wollstadt, M. Bujny, S. Ramnath, J. J. Shah, D. Detwiler, and S. Menzel, "CarHoods10k: An Industry-grade Data Set for Representation Learning and Design Optimization in Engineering Applications," *IEEE Trans. Evol. Comput.*, pp. 1–1, 2022.

[10] S. Ramnath, J. J. Shah, P. Wollstadt, M. Bujny, S. Menzel, and D. Detwiler, "OSU-Honda automobile hood dataset (CarHoods10k)," in *Dryad Dataset*, 2022.

[11] S. Ramnath *et al.*, "Automatically Generating 60,000 CAD Variants for Big Data Applications," in *International Design Engineering Technical Conferences and Computers and Information in Engineering Conference*, 2019.

[12] S. Ramnath, P. Haghighi, J. Ma, J. J. Shah, and D. Detwiler, "Design Science meets Data Science: Curating Large Design Datasets for Engineered Artifacts," in *International Design Engineering Technical Conferences and Computers and Information in Engineering Conference*, 2020.

[13] A. Adrian, S. Ramnath, S. C. Sunkara, Y. Korkolis, J. K. Davidson, and J. J. Shah, "Curating Datasets of Flexible Assemblies to Predict Spring-Back Behavior for Machine Learning Purposes," in *Volume 2: Manufacturing Processes; Manufacturing Systems*, 2022, vol. 13, no. 1, pp. 104–116.

[14] A. Adrian, "Automation and Validation of Big Data Generation via Simulation Pipeline for Flexible Assemblies," The Ohio State University, 2022.

[15] S. C. Liu, S. J. Hu, and T. C. Woo, "Tolerance analysis for sheet metal assemblies," *J. Mech. Des. Trans. ASME*, vol. 118, no. 1, pp. 62–67, 1996.

[16] J. A. Camelio and S. J. Hu, "Compliant assembly variation analysis using components geometric covariance," *ASME Int. Mech. Eng. Congr. Expo. Proc.*, pp. 431–437, 2002.

[17] K. G. Merkley, K. W. Chase, and E. Perry, "An Introduction to Tolerance Analysis of Flexible Assemblies," 1996.

[18] D. J. Ceglarek and J. Shi, "Tolerance analysis for sheet metal assembly using a beam-based model," in *American Society of Mechanical Engineers, Design Engineering Division (Publication) DE*, 1997, vol. 94, pp. 153–159.

[19] A. J. Mortensen, "An Integrated Methodology for Statistical Tolerance Analysis of Flexible Assemblies," Brigham Young University, 2002.

[20] M. R. Tonks and K. W. Chase, "Covariance Modeling Method for Use in Compliant Assembly Tolerance Analysis," in *Volume 1: 30th Design Automation Conference*, 2004, pp. 49–55.

[21] M. R. Tonks, K. W. Chase, and C. C. Smith, "Predicting Deformation of Compliant Assemblies Using Covariant Statistical Tolerance Analysis," in *Models for Computer*

Aided Tolerancing in Design and Manufacturing, Dordrecht: Springer Netherlands, pp. 321–330.
[22] ASME Y14.5, "Dimensioning and Tolerancing," *NY Am. Soceity Mech. Eng.*, p. 704, 2009.
[23] A. Stockinger, S. Wittmann, M. Martinek, H. Meerkamm, and S. Wartzack, "Virtual assembly analysis: Standard tolerance analysis compared to manufacturing simulation and relative positioning," *11th Int. Des. Conf. Des. 2010*, pp. 1421–1430, 2010.
[24] S. Moos and E. Vezzetti, "Compliant assembly tolerance analysis: guidelines to formalize the resistance spot welding plasticity effects," *Int. J. Adv. Manuf. Technol.*, vol. 61, no. 5–8, pp. 503–518, Jul. 2012.
[25] A. Hashemian and B. M. Imani, "A new quality appearance evaluation technique for automotive bodies including effect of flexible parts tolerances," *Mech. Based Des. Struct. Mach.*, vol. 46, no. 2, pp. 157–167, Mar. 2018.
[26] V. Viswanathan, B. Kinsey, and J. Cao, "Experimental Implementation of Neural Network Springback Control for Sheet Metal Forming," *J. Eng. Mater. Technol.*, vol. 125, no. 2, pp. 141–147, Apr. 2003.
[27] J. Y. Lee, M.-G. Lee, and F. Barlat, "Evaluation of Constitutive Models for Springback Prediction in U-draw/bending of DP and TRIP Steel Sheets," in *AIP Conference Proceedings*, 2011, pp. 571–578.
[28] P. C. Hansen, V. Pereyra, and G. Scherer, *Least squares data fitting with applications*, vol. 9781421408. 2012.
[29] V. Srinivasan, C. M. Shakarji, and E. P. Morse, "On the Enduring Appeal of Least-Squares Fitting in Computational Coordinate Metrology," *J. Comput. Inf. Sci. Eng.*, vol. 12, no. 1, Mar. 2012.
[30] D. Eberly, "Least squares fitting of data." [Online]. Available: https://www.cse.iitb.ac.in/~cs749/spr2017/handouts/eberly_least_square_fitting.pdf.
[31] C. R. Harris *et al.*, "Array programming with NumPy," *Nature*, vol. 585, no. 7825, pp. 357–362, Sep. 2020.
[32] G. Mills, *Introduction to Linear Algebra*. Cambridge University Press, 2017.
[33] P. Mohan, P. Haghighi, J. J. Shah, and J. K. Davidson, "Development of a library of feature fitting algorithms for CMMs," *Int. J. Precis. Eng. Manuf.*, vol. 16, no. 10, pp. 2101–2113, Sep. 2015.
[34] P. Virtanen *et al.*, "SciPy 1.0: fundamental algorithms for scientific computing in Python," *Nat. Methods*, vol. 17, no. 3, pp. 261–272, Mar. 2020.